Emergence of hexatic and threefold hidden order in two-dimensional smectic liquid crystals: A Monte Carlo study

Farhad Shahbazi[1,*] and Rasool Ghanbari[2]
[1]*Department of Physics, Isfahan University of Technology, 84156, Isfahan, Iran*
[2]*Department of Physics, Islamic Azad University, Majlesi Branch, 86315/111, Isfahan, Iran*
(Received 1 October 2005; published 16 August 2006)

Using a high resolution Monte Carlo simulation technique based on a multihistogram method and cluster algorithm, we have investigated the critical properties of a coupled XY model, consisting of a sixfold symmetric hexatic and a hidden order parameter of threefold symmetry in two dimensions. The simulation results demonstrate a series of continuous transitions in which both kinds of orderings are established simultaneously. It is found that the specific-heat anomaly exponents for some regions in coupling constants space are in excellent agreement with the experimentally measured exponents extracted from heat-capacity data near the smectic-*A*–hexatic-*B* transition of two-layer free standing films.

DOI: 10.1103/PhysRevE.74.021705 PACS number(s): 61.30.−v, 64.70.Md

I. INTRODUCTION

The mysterious critical properties of bulk and thin film liquid crystals at phase transition between smectic-*A* (Sm*A*) phase with liquid like in-plane behavior and hexatic-*B* (Hex*B*) phase with long-range bond orientational order but short range in-plane positional order, have remained as a challenge for experimental and theoretical physicists after about 25 years.

The concept of hexatic phase was first introduced in two-dimensional (2D) melting theory by Kosterlitz, Thouless, Halperin, Nelson, and Young (KTHNY) [1–3]. According to this theory, a two-dimensional solid would melt, via two Kosterlitz-Thouless (KT)-type transitions, through an intermediate hexatic phase into the isotropic phase. This hexatic phase displays short-range positional order, but quasi-long-range bond-orientational order, which is different from the true long-range bond-orientational and quasi-long-range positional order in 2D solid phases. It is known that for two-dimensional systems, the transition from the isotropic liquid to hexatic phase could be either a KT transition or a first order transition [4]. The three-dimensional hexatic phase was first proposed by Birgeneau and Lister as a stack of weakly coupled 2D hexatic layers, where the interlayer interactions make the quasi-long-range order of two-dimensional layers truly long ranged [5].

The first signs for the existence of the hexatic phase in three-dimensional systems were observed in x-ray diffraction study of liquid crystal compound 65OBC(*n*-alkyl-4-*m*-alkoxybiphenyl-4-carboxylate,$n=6,m=5$) [6,7], where a hexagonal pattern of diffuse spots was found in intensity of scattered x rays. In addition to this hexagonal pattern, it was also found that some broader peaks appeared in the diffracted intensity which indicate the onset of another ordering. These broad peaks are related to packing of molecules according to the herringbone structure perpendicular to the smectic layer stacking direction, although the range of herringbone ordering was not determined by a detailed investigation. The accompanying of the long-range hexatic and herringbone orders make this phase a physically rich phase which is simply called hexatic-*B* (Hex*B*) phase. When temperature is decreased, the Hex*B* phase transforms via a first order phase transition into the crystal-*E* (Cry*E*) phase, which is a 3D plastic crystal exhibiting long-range herringbone orientational ordering. Subsequently, it was found that other components in *nm*OBC homologous series (such as 37OBC and 75OBC) and a number of binary mixtures of *n*-alkyl-4′-*n*-decycloxybiphenyl-4-carboxilate [*n*(10)OBC] with *n* ranging from 1 to 3 also represent sm*A*–Hex*B* transition. In summary most of the *nm*OBC homologous series undergo the bulk transition sequences, isotropic-Sm*A*–Hex*B*–Cry*E*–Cry*K*, where Cry*K* is the rigid crystal structure, stable at room temperature.

The sixfold symmetry of hexatic phase suggests that bond-orientational order parameter be defined by $\Psi_6=|\Psi_6|\exp(i6\psi_6)$ describing the sixfold azimuthal modulation. The U(1) symmetry of the Ψ_6 implies that the Sm*A*–Hex*B* transition is a member of the XY universality class. However, heat capacity measurements on bulk samples of 65OBC [7,8] and other calorimetric studies on many other components in the *nm*OBC homologous series [7,9] have yielded very sharp specific heat anomalies near the Sm*A*–Hex*B* transition with no detectable thermal hystersis and with a very large value for the heat capacity critical exponent, $\alpha\approx 0.6$. These results indicate that this is a continuous (second order) phase transition, but not belonging to the 3D XY universality class, for which the specific heat critical exponent is nearly zero ($\alpha\approx -0.007$ [10]). On the other hand, the other static critical exponents determined from thermal conductivity ($\eta=-0.19$) and birefringence experiments ($\beta=0.19$) [7], all differ from the 3D XY values, indicating a novel phase transition with probably a new universality class. More recent calorimetric studies of 65OBC [11] and 3(10)OBC [12], however, suggest that the Sm*A*–Hex*B* transitions in these compounds are weakly first order which, as well, are in contrast with the assumption of XY universality. There are also some liquid crystal compounds (i.e., PHOAB, 54COOBC, FRFL6, PIR5) which exhibit phase sequences isotropic-Sm*A*–Hex*B*–Cry*B* with no sign of herringbone ordering in

*Electronic address: shahbazi@cc.iut.ac.ir

transition from hexatic to plastic crystal-*B*. For these compounds the Sm*A*–Hex*B* transition has been found to be first order (for a review see [13]).

This unusual behavior also occurs in two-dimensional liquid crystal compounds undergoing bulk hexatic transitions. The heat capacity measurement studies of (truly two-dimensional) two-layer freestanding films of different *nm*OBC compounds result in a second order Sm*A*–Hex*B* transition, with a diverging specific-heat anomaly described by exponent $\alpha=0.31\pm0.03$ [7,14–16]. This is obviously in contrast with the usual broad and nonsingular specific-heat hump of the KT transition far above T_c, predicted in two-dimensional melting theory. On the other hand, electron diffraction studies on *nm*OBC compound films revealed weak herringbone orders in hexatic phases, suggesting that the Sm*A*–Hex*B* transition cannot be described simply by a unique XY order parameter and the discrepancy between the experimental and two-dimensional melting theory could be due to the presence of herringbone order in addition to the bond-orientational order in such compounds.

In the light of these observations, Bruinsma and Aeppli [17] formulated a Ginzburg-Landau theory that included both hexatic and herringbone orders. There are three inequivalent orientations for the herringbone pattern on a triangular lattice, so the herringbone order parameter should be threefold symmetric. Nevertheless, the broadness of x-ray diffracted peaks associated to herringbone order made Bruinsma and Aeppli to consider it short-ranged and associate an XY order parameter with twofold symmetry for herringbone ordering $[\Phi_2=|\Phi_2|\exp(i2\phi_2)]$. Based on symmetry arguments, they also made a minimal coupling between the hexatic and herringbone order parameters as $V_{hex\text{-}her}=h\,\mathrm{Re}(\Psi_6^*\Phi_2^3)$. Microscopically, the origin of this coupling could be the anisotropy presented in liquid crystals molecular structures [18,19]. In the mean field approach their results indicate that the Sm*A*–Hex*B* transition should be continuous. However, one-loop renormalization calculations show that short-range molecular herringbone correlations coupled to the hexatic ordering drive this transition to a first order one, which becomes second order at a tricritical point [17]. Therefore they concluded that the occurrence of phase transition near the tricritical points, with heat capacity exponent $\alpha=0.5$, would be a good explanation for the large heat capacity exponents observed in the experiments. Recently, the RG calculation of the BA model has been revised in [20] which resulted in finding another nontrivial fixed point missed in the original work of Bruinsma and Aeppli; but it has been shown that this new fixed point is unstable in one loop level (order of ϵ), which refuses this fixed point to represent a novel phase transition. Indeed, the limitations of RG methods which mostly rely on perturbation expansions make them insufficient for accessing the strong coupling regimes where one expects some kind of new treatments to appear. For this purpose, the numerical simulations would be useful.

The first numerical simulations for investigating the nature of the Sm*A*–Hex*B* transition in 2D systems have been done by Jiang *et al.* who have used a model consisting of a 2D lattice of coupled XY spins based on the BA Hamiltonian in the strong coupling limit [21,22]. Their simulation results suggest the existence of a new type of phase transition in which two different orderings are simultaneously established through a continuous transition with heat capacity exponent $\alpha=0.36\pm0.05$, in good agreement with experimental values. Recently, we have carried out a high-resolution Monte Carlo simulation, based on the multihistogram method, on the BA model in three dimensions. Our results revealed the existence of a tricritical point on the transition line between Sm*A* and hexatic+herringbone phases, but not any tricritical point on the isotropic–hexatic transition line [23].

Although the occurrence of Sm*A*–Hex*B* in the vicinity of a tricritical point might be a convincing reason for its observed large heat capacity exponents, some other questions remain unsolved. One question is that why seven different liquid crystal compounds *nm*OBC and five binary mixtures *n*(10)OBC, with very different Sm*A*–Hex*B* temperature ranges (which effect the coupling of two order types) yield approximately the same value $\alpha\approx0.6$ and should all be in the immediate vicinity of a particular thermodynamic point. For example, the herringbone peaks observed in x-ray diffraction studies of 75OBC are weaker than those of 65OBC, hence if 65OBC is near a tricitical point then 75OBC should be further removed from this point. Yet the same specific-heat critical exponents have been obtained for these two compounds. The other problem concerns the mixture of 3(10)OBC (3-alkyl-4′-*n*-decycloxybiphenyl-4-carboxilate) and PHOAB (4-propionyl-4′-*n*-heptanoyloxyazo-benzene) compounds with PHOAB concentration between 30% and 70%, for which one expects very small herringbone fluctuations (because of large Hex*B* temperature range) and therefore the Sm*A*–Hex*B* transition must be second order but first order transitions were found for these mixtures. On the other hand, the first order transition observed in the bulk sample of compounds exhibiting Sm*A*–Hex*B*–Cry*B* and also diverging heat capacity in free-standing 54COOBC films [15,16], despite the absence of herringbone ordering, put the hexatic-herringbone coupling idea, as an explanation for the unexpected critical behavior of Sm*A*–Hex*B* transitions, against serious challenges.

Because of the above reasons, some other theoretical models have been proposed addressing the coupling of hexatic order parameter and positional density ρ [24,25], smectic layer fluctuations u [26], and also tilt [27]. Nevertheless, none of these models has been able to explain the detailed critical behavior near the Sm*A*–Hex*B* transition. Another possibility is the coupling hexatic ordering with some hidden order parameters (undetectable in experiments), rather than herringbone order. A reasonable choice could be the coupling of hexatic order parameter with sixfold symmetry with another XY order parameter with a symmetry different from twofold symmetry of short-range herringbone ordering suggested by Bruinsma and Aeppli.

The coupled XY models have been widely used for studying the critical properties of two-dimensional systems in which the ground states exhibit both continuous and discrete degeneracy simultaneously. Some examples of such systems are the fully frustrated XY models [28] which as a realization one can mention a Josephson junction array in a transverse magnetic field with half a flux quantum per plaquette, the antiferromagnetic XY model on a triangular lattice [29], the double-layer XY model [30], and the helical XY model [31].

The unusual critical behaviors have also been observed in XY models with mixed action [32] and coupling of XY model with Ising model [33].

In view of the above remarks, we were motivated to investigate the critical properties of a two-dimensional coupled XY model consisting of a hexatic order parameter with sixfold symmetry and another XY order parameter with threefold symmetry as an alternative model for describing the SmA–Hex$B$ transition. For this purpose we employ a high-resolution Monte Carlo technique to derive the critical temperatures and the critical exponents of this model over some ranges of coupling constants, and will show that for some values of coupling constants the heat-capacity anomaly exponents, extracted from simulation, are very close to the experimental values obtained from high-resolution ac calorimetry on the thin films of some liquid crystal compounds exhibiting two-dimensional SmA–Hex$B$ transition.

The rest of this paper is organized as follows. In Sec. II we introduce a model Hamiltonian and give a brief introduction to Wolff's embedding method for reducing the critical slowing down and correlation between the measurements, the optimized Monte Carlo method based on multiple histograms, and also some methods for analyzing the Monte Carlo data to determine the order of transitions, critical temperatures, and critical exponents. The simulation results and discussion are given in Sec. III and conclusions will appear in Sec. IV.

II. MONTE CARLO SIMULATION

A. Model

Recalling the sixfold symmetry of hexatic order and threefold symmetry of the underlying hidden order, the Hamiltonian which describes both orderings ought to be invariant with respect to the transformation $\Phi \rightarrow \Phi + n(2\pi/3)$ and $\Psi \rightarrow \Psi + m(2\pi/6)$ (where n and m are integers) and also under any global rotation in the xy plane. Thus to lowest order in Ψ and Φ, one can write the following Hamiltonian for this model:

$$H = -J_1 \sum_{\langle ij \rangle} \cos(6\Psi_i - 6\Psi_j) - J_2 \sum_{\langle ij \rangle} \cos(3\Phi_i - 3\Phi_j) - J_3 \sum_i \cos(6\Psi_i - 6\Phi_i), \quad (1)$$

which by redefinitions $\Psi' = 6\Psi$ and $\Phi' = 3\Phi$ we reach the following form for the Hamiltonian:

$$H = -J_1 \sum_{\langle ij \rangle} \cos(\Psi_i' - \Psi_j') - J_2 \sum_{\langle ij \rangle} \cos(\Phi_i' - \Phi_j') - J_3 \sum_i \cos(\Psi_i' - 2\Phi_i'), \quad (2)$$

where the coefficients J_1 and J_2 are the nearest-neighbor coupling constants for the bond-orientational order (Ψ) and hidden order (Φ), respectively. The coefficient J_3 denotes the coupling strength between these two types of order at the same 3D lattice site. We are interested in situations in which Ψ and Φ are coupled relatively strongly. Therefore for the beginning we fixed $J_3 = 2.0$, larger than both J_1 and J_2 for all the simulations. Assuming J_1 much larger than $J_2 (J_1 \gg J_2)$ for sufficiently high temperatures (say $T > J_3$), the system is in a completely disordered phase. For $T_{c1} < T < J_3$, the system remains disordered but the phases of the two order parameters become coupled through the coupling term J_3; because of the XY symmetry of bond-orientational order, for $T_{c2} < T < T_{c1}$, the hexatic order is first established through a KT transition and one would expect the ordered state to be correspondent to $\Psi_i \approx \Psi_j$ for all sites i and j, producing two degenerate minima for the free energy. So for this temperature range the above Hamiltonian describes a system with the symmetry of the 2D-Ising model and then the transition between the pure hexatic ($\Psi \neq 0$, $\Phi = 0$) and the locked phase (hexatic plus threefold ordering) ($\Psi \neq 0$, $\Phi \neq 0$) should be Ising-like at T_{c2} with critical properties of the 2D-Ising model. Thus for $J_2 \ll J_1 < J_3$ the model exhibits a KT transition at $T_{c1} \sim \frac{\pi J_1}{2}$ and an Ising-like transition upon decreasing the temperature down to $T_{c2} \sim 2.7 J_2$ ($k_B = 1$). For $J_2 \approx \frac{\pi J_1}{5.4} \approx 0.58 J_1$, the two transition temperatures turn out to be equal and so a single transition occurs between disordered and locked phases in which two orderings would be established simultaneously.

For $0.58 J_1 < J_2 < J_3$ the threefold order would establish first and cause the correspondent field Φ to take nearly the same value for all sites. Because of this, the coupling term J_3 acts like a field on Ψ and so the hexatic order parameter takes a nonzero value. So for this range of coupling constants the threefold ordering will induce hexatic order at the same time.

Using the renormalization group analysis, the critical properties of Hamiltonian given by Eq. (2) have been studied by Granato and Kosterlitz in [34], where they have obtained the phase diagram consisting of the three possible phases mentioned above. They also argued that the transition from ordered to partially ordered is continuous while the transition from disordered to fully locked ordered phase with long-range Ising state and algebraic XY order is weakly first order.

To obtain a qualitative picture of the transitions and also the approximate location of the critical points, we first set some low resolution simulations. The simulations were carried out using the standard Metropolis spin-flipping algorithm with lattice size $L = 20 \times 20$. During each simulation step, the angles Ψ_i and Φ_i were treated as unconstrained, continuous variables. The random-angles rotations ($\Delta\Psi_i$ and $\Delta\Phi_i$) were adjusted in such a way that roughly 50% of the attempted angle rotations were accepted. To ensure thermal equilibrium, 100 000 Monte Carlo steps (MCS) per spin were used for each temperature and 200 000 MCS were used for data collection. The basic thermodynamic quantities of interest are the specific heat $c = (\langle E^2 \rangle - \langle E \rangle^2)/(T^2 L^2)$, the threefold order parameter $M = L^{-2}\{[\Sigma_i \cos(\Phi_i)]^2 + [\Sigma_i \sin(\Phi_i)]^2\}$ and the susceptibility $\chi = (\langle M^2 \rangle - \langle M \rangle^2)/(TL^2)$.

We have obtained the specific heat, susceptibility, and order parameter data as a function of temperature, shown in Figs. 1–3, for $J_1 = 1.0$, $J_2 = 0.5$, 0.6, 0.8, 1.0, and $J_3 = 2.0$. From the preceding discussion, it is clear that the small broad peaks near $T = 1.1$ in Figs. 1 and 2 signal the XY transition due to the J_1 term, while the sharp peak located at $T \sim 0.9$ is

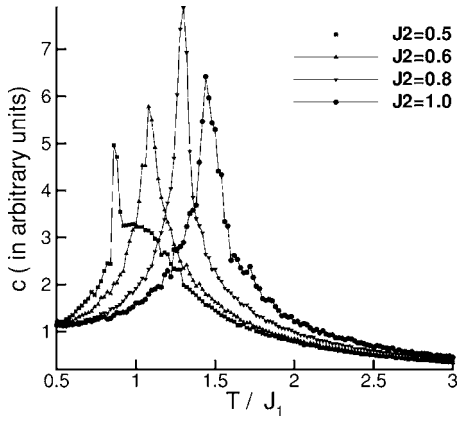

FIG. 1. Temperature dependence of specific-heat for $J_1=1.0$, $J_3=2.0$, and $J_2=0.5$, 0.6, 0.8, and 1.0.

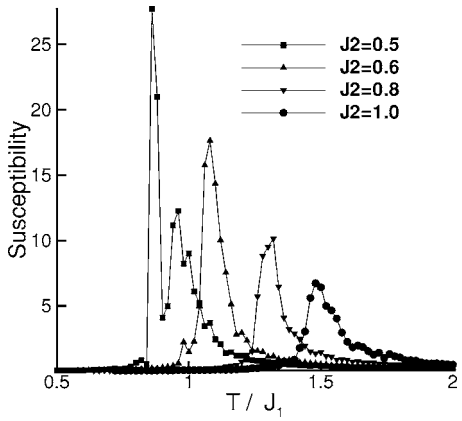

FIG. 3. Temperature dependence of susceptibility for $J_1=1.0$, $J_3=2.0$, and $J_2=0.5$, 0.6, 0.8, and 1.0.

expected to signal a transition into the state of 2D-Ising symmetry. For $J_2>0.6$, as already mentioned, only one sharp peak is observed in the specific-heat and susceptibility data which verifies our argument that for these values of J_2, the transition from disordered to threefold ordered phase simultaneously induces hexatic ordering.

B. Wolff's embedding trick

One important problem in Monte Carlo simulation, especially for large systems, is critical slowing down which is a major source of errors in measurements. To overcome the critical slowing down we used Wolff's embedding technique [35]. This method is based on the cluster algorithm which originally proposed by Swendsen and Wang for the Potts model [36]. In the Swendsen and Wang cluster algorithm a configuration of activated bonds is constructed from the spin configuration and after the clusters of spins are formed from configuration of bonds the spin configuration is updated by assigning a randomly new spin value to each cluster and then the same value is given to all spins in the same cluster.

Wolff suggested a single-cluster algorithm in the way that only a single cluster grows from a randomly chosen site and then all the spins in the cluster are flipped. This single-cluster algorithm is very successful when applied to the Ising model [37].

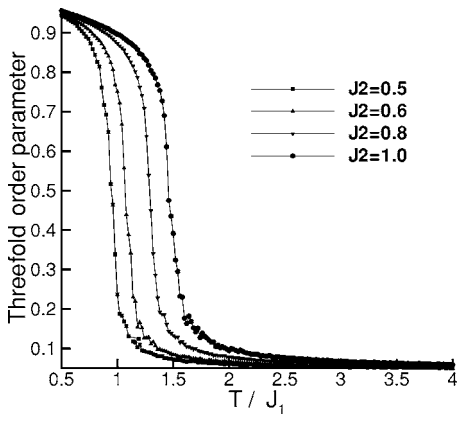

FIG. 2. Temperature dependence of the threefold order parameter for $J_1=1.0$, $J_3=2.0$, and $J_2=0.5$, 0.6, 0.8, and 1.0.

Wolff further developed his technique for spin systems with continuous symmetry by introducing the Ising variable into $O(n)$ ferromagnetic models. Choosing a direction in the spin space at random each spin is projected onto that direction with two components, one perpendicular and the other either parallel or antiparallel to the randomly chosen direction. An Ising model is then constructed by assigning +1 to spins of parallel components and −1 to spins of antiparallel components. The couplings between the nearest-neighbor Ising spins are determined by the products of these parallel and antiparallel components and are therefore random in magnitude but are ferromagnetic. Such a random-bond Ising model can efficiently be simulated with the single-cluster algorithm and the original $O(n)$ model can be updated correspondingly by changing the sign of parallel or antiparallel components of spins in the same cluster [38–40].

For cluster updating of the coupled XY model, we performed the following steps.

(i) Choose a random oriented direction in the two-dimensional system with angle θ respect to the x axis and find the relative rotation of one of the two fields, i.e., hexatic field (Ψ), respect to the randomly chosen direction ($\Psi_i'=\Psi_i-\theta$).

(ii) For each axis direction, generate independent random-bond Ising models for Ψ variables by assigning +1 to each lattice point if $\cos(\Psi_i')>0$ and −1 if $\cos(\Psi_i')<0$.

(iii) For each resultant random-bond Ising model correspondent to hexatic field, choose a lattice site randomly and build a single cluster with a bond-activating probability

$$P_{ij}=1-\exp\{\min[0,-2K_1\cos(\Psi')_i\cos(\Psi')_j]\}, \qquad (3)$$

where $K_1=J_1/T$ and the Boltzamann constant being 1;

(iv) The spins in each cluster feel the effect of Φ fields through coupling term J_3. Once the Ψ cluster is formed, update its configuration by flipping all correspondent embedded Ising variables in each cluster using the Metropolis algorithm. For this purpose consider ΔE as the energy difference of spin flipped and initial configurations for a given cluster in such a way that if $\Delta E<0$ all spins in the cluster

will be flipped ($\Psi_i' \to \pi - \Psi_i'$) and if $\Delta E > 0$ they will be flipped by probability $p = \exp(-K_3 \Delta E)$ in which $K_3 = J_3/T$. Note that in this procedure all Φ variables remain unchanged.

(v) Repeat (ii)–(iv) several times before going to the next step.

(vi) Now fix Ψ variables and repeat steps (ii)–(v) for ϕ variables, noting that in step (iii) K_1 should be changed to $K_2 = J_2/T$.

(vii) Turn to step (i) and choose a new random direction.

This multiple-updating scheme satisfies detailed balance and ergodicity and critical slowing down is reduced dramatically. To improve the quantity of data we combined the above algorithm with the single flip Metropolis method.

All simulations were carried out at five temperatures close to the effective transition points of the square lattices with linear sizes $L = 20$, 24, 28, 32, 36, 40, 50, and 60, by characterizing the corresponding peak position of the specific-heat and finite-lattice susceptibility. In each simulation 1×10^5 cluster updating runs were carried out for equilibration. For data collection, 4×10^5 measurements were made after enough single cluster-updating followed by single flip Metropolis runs are skipped (at least ten) to reduce the correlation between the measurements. Values of total energy and magnetization from each measurement were stored as a data list for histogram analysis.

C. Histogram method

To determine the location of the transition temperatures and other thermodynamic quantities such as specific heat near the transition points we need to use high resolution methods. For this purpose we used the multiple-histogram reweighting method proposed by Ferrenberg and Swendsen [41], which makes it possible to obtain accurate data over the transition region from just a few Monte Carlo simulations. The central idea behind the histogram method is to build up information on the energy probability density function $P_\beta(E)$, where $\beta = 1/T$ is inverse temperature (in units with $k_B = 1$). A histogram $H_\beta(E)$ is the number of spin configurations generated between E and $E + \delta E$. $P_\beta(E)$ is defined as

$$P_\beta(E_i) = \frac{H_\beta(E_i)}{Z_\beta}, \tag{4}$$

where

$$Z_\beta = \sum_i H_\beta(E_i). \tag{5}$$

On the other hand we know that $P_\beta(E_i)$ is proportional to the Boltzmann weight $\exp(-\beta E_i)$ as

$$P_\beta(E_i) = \frac{g(E_i)\exp(-\beta E_i)}{Z_\beta}, \tag{6}$$

in which $g(E_i)$ is the density of states with energy E_i and is independent of temperature. By knowing the probability distributions in a specific temperature, we can derive the density of states and find the probability distribution of energy at any temperature β' as follows:

$$P_{\beta'}(E_i) = \frac{P_\beta(E_i)\exp[(\beta - \beta')E_i]}{\sum_j P_\beta(E_j)\exp[(\beta - \beta')E_j]}. \tag{7}$$

In principle, $P_\beta(E)$ only provides information on the energy distribution of nearby temperatures. This is because the counting statistics in the wings of the distribution $H_\beta(E)$, far from the average energy at temperature T, will be poor.

To improve the estimation for density of states, one can take data at more than one temperature and combine the resultant histograms so as to take the advantages of the regions where each provide the best estimate for the density of states. This method has been studied by Ferrenberg and Swendsen who presented an efficient way for combining the histograms [41]. Their approach relies on first determining the characteristic relaxation time τ_j for the jth simulation and using this to produce a weighting factor $g_j = 1 + 2\tau_j$. The overall probability distribution at coupling $K = \beta J$ obtained from n independent simulation, each with N_j configurations, is then given by

$$P_K(E) = \frac{\left[\sum_{j=1}^{n} g_j^{-1} H_j(E)\right] e^{-KE}}{\sum_{j=1}^{n} N_j g_j^{-1} e^{-K_j E - f_j}}, \tag{8}$$

where $H_j(E)$ is the histogram for the jth simulation and the factors f_j are chosen self-consistently using Eq. (8) and

$$e^{f_j} = \sum_E P_{K_j}(E). \tag{9}$$

Thermodynamic properties are determined, as before, using this probability distribution, but now the results would be valid over a much wider range of temperatures than for any single histogram. In addition, this method gives an expression for the statistical error of $P_K(E)$ as

$$\delta P_K(E) = \left[\sum_{j=1}^{n} g_j^{-1} H_j(E)\right]^{-1/2} P_K(E), \tag{10}$$

from which it is clear that the statistical error will be reduced when more MC simulations are added to the analysis.

To deal with thermodynamic quantities other than the energy, one can choose to work with energy probability distribution and microcanonical averages of the quantities of interest. This leads to optimized use of computer memory. The microcanonical average of a given quantity M, which is a function of energy, can be calculated directly as

$$M(E) = \frac{\sum_t M_t \delta_{E_t,E}}{\sum_t \delta_{E_t,E}}, \tag{11}$$

from which the canonical average of M can be obtained as a function of T:

$$\langle M\rangle = \frac{\sum_E M(E)P(E,T)}{\sum_E P(E,T)}. \tag{12}$$

The temperature dependence of thermodynamic quantities was determined by the optimized multiple-histogram method. For all system sizes, histograms obtained from simulations overlap sufficiently on both sides of the critical point so that the statistical uncertainty in the wing of the histograms, near the critical point, may be suppressed by using the optimized multiple-histogram method. Therefore the locations and magnitudes of the extrema of the thermodynamic quantities can be determined accurately to extract the critical temperature and static critical exponents from the finite-size scaling behavior.

D. Determination of T_c and static critical exponents

In order to determine the critical temperature in the infinite lattice sizes as well as the critical exponents, we use the finite-size scaling theory [42]. According to the finite-size scaling theory, the free energy density can be divided into a singular part f_s and a background f_{ns} which is nonsingular as

$$f(t,h;L) = f_s(t,h;L) + f_{ns}(t,L), \tag{13}$$

where $t=(T-T_c)/T_c$ is the reduced temperature for a sufficiently large system at a temperature T close enough to the infinite lattice critical point T_c and h is the external ordering field. Using the periodic boundary conditions makes the nonsingular part size independent, leaving only the singular part of free energy for studying the critical properties of the system. The singular part is described phenomenologically by a universal scaling form

$$f(t,H;L) = L^{-d}Y(tL^{y_t},hL^{y_h}) + \cdots, \tag{14}$$

where d is the spatial dimension of the system and y_t and y_h are related to static critical exponents as $y_t=1/\nu$ and $y_h=\frac{\beta\delta}{\nu}$. The scaling form for various thermodynamic quantities can be obtained from proper derivations of the free energy density. Some of them such as magnetization density, susceptibility, and specific heat in zero field are

$$m \approx L^{\beta/\nu}\mathcal{M}(tL^{1/\nu}), \tag{15}$$

$$\chi \approx L^{\gamma/\nu}\mathcal{K}(tL^{1/\nu}), \tag{16}$$

$$c \approx c_\infty(t) + L^{\alpha/\nu}\mathcal{C}(tL^{1/\nu}), \tag{17}$$

in which α, β, γ, and δ are static critical exponents. Equations (15)–(17) are used to estimate the critical exponents. But before dealing with the critical exponents we should first determine the critical temperature accurately.

The logarithmic derivatives of total magnetization (mL^d) are important thermodynamic quantities for studying critical phenomena and very useful to high accurate estimation of the critical temperature T_c and the critical exponent ν [39]. For example, defining the following quantities:

$$V_1 \equiv 4[M^3] - 3[M^4], \tag{18}$$

$$V_2 \equiv 2[M^2] - [M^4], \tag{19}$$

$$V_3 \equiv 3[M^2] - 2[M^3], \tag{20}$$

$$V_4 \equiv (4[M] - [M^4])/3, \tag{21}$$

$$V_5 \equiv (3[M] - [M^3]\ /2, \tag{22}$$

$$V_6 \equiv 2[M] - [M^2], \tag{23}$$

where $M=mL^d$ is the total magnetization of the system and

$$[M^n] \equiv \ln\frac{\partial\langle M^n\rangle}{\partial T}. \tag{24}$$

From Eq. (15) it is easy to show that

$$V_j \approx (1/\nu)\ln L + \mathcal{V}_j(tL^{1/\nu}), \tag{25}$$

for $j=1,2,\ldots,6$. At the critical temperature ($t=0$) the $\mathcal{V}_j$ should be constants independent of the system size L. As we will see it gives us a very accurate tool to estimate both the critical temperature and the correlation length exponent ν independently with high precision.

E. Order of the transition

To determine the order of transitions, we used Binder's forth energy cumulant defined as

$$U_L = 1 - \frac{\langle E^4\rangle}{3\langle E^2\rangle}. \tag{26}$$

It has been shown that this quantity reaches a minimum at the effective transition temperature $T_c(L)$ whose size dependence is given by [43–45]

$$U_{\min}(L) = U^* + BL^{-d} + O(L^{-2d}), \tag{27}$$

where

$$U^* = \frac{2}{3} - (e_1/e_2 - e_2/e_1)^2/12. \tag{28}$$

The quantities e_1 and e_2 are the values of energy per site at the transition point of a first order phase transition and d is the spatial dimension of the system ($d=2$ in our simulation). Hence for the continuous transitions for which there is no latent heat ($e_1=e_2$), in the limit of infinite system sizes, $U_{min}(L)$ tends to the value U^* equal to 2/3. For the first-order transitions, however, $e_1 \neq e_2$ and then U^* reaches a value less than 2/3 in the limit $L\to\infty$. This method is actually a test for the Gaussian nature of the probability density function $P(E)$ at T_c. For a continuous transition, $P(E)$ is expected to be Gaussian at, as well as away from, T_c. For a first-order transition, $P(E)$ will be double peaked in infinite lattice size limit, hence deviation from being Gaussian causes the minimum of U_L to tend to U^* which is less than 2/3 as $L\to\infty$. This method is very sensitive, in a sense that small splitting in $P(E)$ for the infinite system that does not result in a double peak for small lattices can be detected.

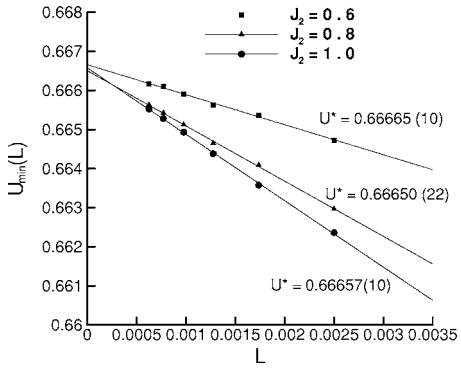

FIG. 4. Size dependence of binder fourth energy cumulant minima, calculated by optimized reweighting for $J_1=1.0$, $J_3=2.0$, and $J_3=0.6$, 0, 8, and 1.0. Solid lines represent fits to Eq. (27). Error bars are less than the size of the points.

III. RESULTS AND DISCUSSION

We are interested in investigating those regions in coupling constants space for which the two kinds of ordering establish together, so we limit ourselves to $\frac{J_2}{J_1}>0.6$. Fixing $J_3=1.0$ and $J_3=2.0$ we start to get data for $J_2=0.6$,0.7,0.8,0.9, and 1.0.

First of all we deal with the order of transitions. Employing the forth Binder energy cumulant method, discussed in the previous section, we found that the order of transition for all values of $0.6\leqslant J_2\leqslant 1.0$ are second order in contrast to [34]. For example, we have plotted the size dependence of minimum values of U_L $[U_{min}(L)$vs $L^{-2}]$ for $J_2=0.6$, 0.8, and 1.0 in Fig. 4. As can be seen from this figure, the asymptotic values of U^* for all the J_2's are equal to 2/3 within the errors of simulations. This indicates that the transitions are continuous for this range of couplings.

After determining the order of transitions we proceed to estimate the critical temperatures and the critical exponents, using the finite-size scaling. The analysis discussed in Sec. II D provides a way to determine both ν and T_c, simultaneously. For this purpose, using Eq. (25) one can find the slope of quantities V_1 to V_6 [Eqs. (18)–(23)] versus ln(L) for

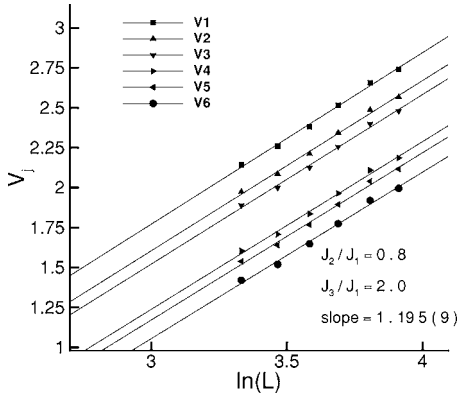

FIG. 5. Dependence of quantity V_j (see the text) vs logarithm of L for $J_1=1.0$, $J_3=2.0$, and $J_2=0.8$ at $T=1.258$. The solid lines represent linear fits to Eq. (25). All straight lines have the same slope 1.195.

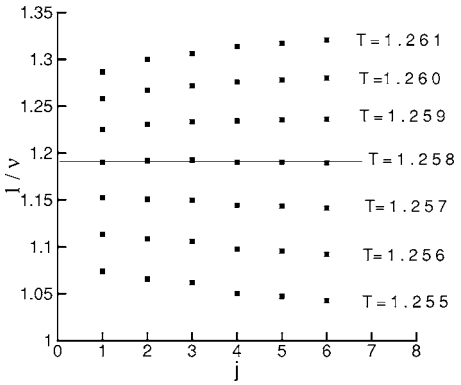

FIG. 6. Scanning results for the dependence of quantity V_j vs j for $J_1=1.0$, $J_3=2.0$, and $J_2=0.8$. The horizontal line is drawn at $1/\nu=1.195$.

the region near the critical point. Scanning over the critical region and looking for a quantity-independent slope gives us both the critical temperature T_c and the correlation length exponent ν with high precision. Figures 5 and 6 give the examples of such an effort for the set of the couplings ($J_1=1.0$, $J_2=0.8$, $J_3=2.0$). From both figures we estimate that $\nu=0.837(5)$ and $T_c=1.157(1)$. The linear fits to the data in Fig. 5 has been obtained by the linear least-squares method. The similar procedure for couplings set ($J_1=1.0$, $J_2=1.0$, $J_3=2.0$), shown in Fig. 7 gives $\nu=1.01(3)$ and $T_c=1.051(1)$.

Once ν and T_c are determined accurately, we can extract other static critical exponents related to the order parameter (β) and susceptibility (γ). The ratio β/ν can be estimated by using the size dependence of the order parameter at the critical point given by Eq. (15). Figures 8 and 9 are log-log plots of the size dependence of the order parameter corresponding to field Φ for $J_2=0.6$ and $J_2=0.8$, respectively. From these figures the ratio β/ν can be estimated as the slope of the straight lines fitted to the data according to Eq. (15). We then have $\beta/\nu=0.143(8)$ for $J_2=0.6$ and $\beta/\nu=0.169(6)$ for $J_2=0.8$ and therefore $\beta=0.144(8)$ for $J_2=0.6$ and $\beta=0.142(5)$ for $J_2=0.8$.

Accordingly, from Eq. (16) it is clear that the peak values of the finite-lattice susceptibility $[\chi=(\langle M^2\rangle-\langle M\rangle^2)/(TL^2)]$

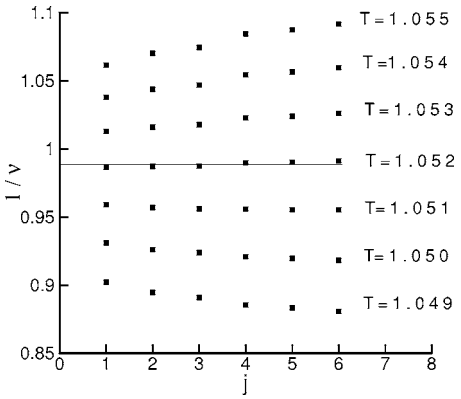

FIG. 7. Scanning results of quantity V_j for $J_1=1.0$, $J_3=2.0$, and $J_2=0.6$. The horizontal line is drawn at $1/\nu=0.99$.

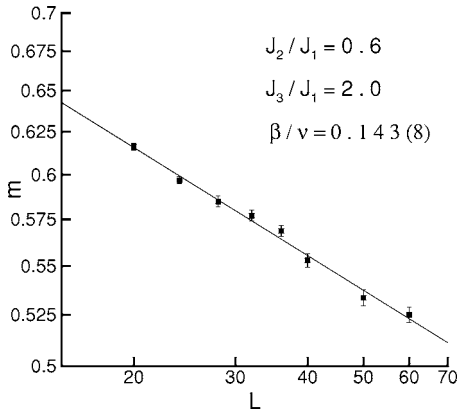

FIG. 8. Log-log plot of order parameter vs the linear size of the lattice L at $T_c=1.052$ for $J_1=1.0$, $J_3=2.0$, and $J_2=0.6$. The solid line is obtained by fitting the data to Eq. (15).

and the magnitude of the true susceptibility at T_c (the same as χ with $\langle m\rangle=0$) are asymptotically proportional to $L^{\gamma/\nu}$. So the slope of a straight line fitted linearly to the log-log plot of these two quantities versus linear size of the lattices can be calculated to estimate the ratio γ/ν. Such plots have been depicted in Figs. 10 and 11 for $J_2=0.6$ and $J_2=0.8$, respectively. In Fig. 10, the slope of the bottom straight line (finite-lattice susceptibility) is 1.726(8) from the linear fit and the slope for the top one is 1.709(7), where the error includes the uncertainty in the slope resulting from uncertainty in our estimate for T_c. The ratio γ/ν obtained from the average of two slopes is 1.717, therefore knowing the value of $\nu=1.01(3)$ one gets $\gamma=1.73(6)$ for $J_2=0.6$ and $J_3=2.0$. Similarly for $J_2=0.8$, depicted in Fig. 11, the slope of the bottom straight line (finite-lattice susceptibility) is 1.637(5) from the linear fit, while for the top one is 1.656(7), so the ratio γ/ν obtained from the average of the slopes is 1.656(9) which results in $\gamma=1.39(1)$ for $J_2=0.8$ and $J_3=2.0$.

The above procedure has been applied for other values of J_2 and the critical temperatures and critical exponents are listed in Table. I. In this table, the critical exponents α, δ, and η have been calculated using scaling laws:

$$\alpha = 2 - d\nu, \tag{29}$$

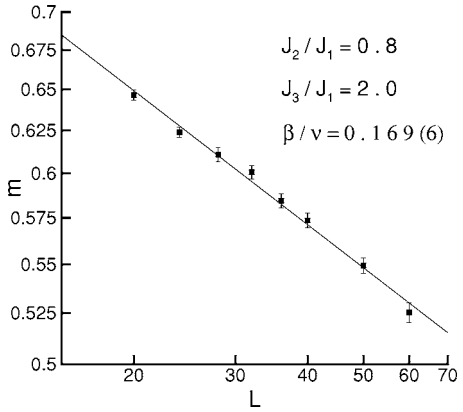

FIG. 9. Log-log plot of order parameter vs the linear size of the lattice L at $T_c=1.257$ for $J_1=1.0$, $J_3=2.0$, and $J_2=0.8$. The solid line is obtained by fitting the data to Eq. (15).

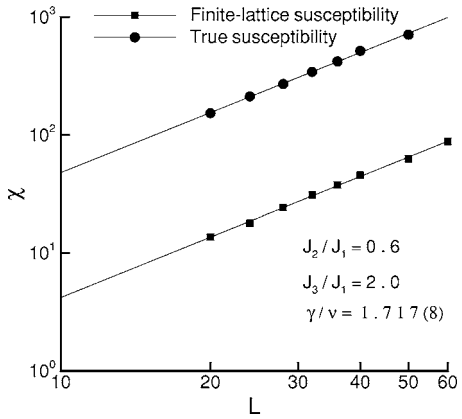

FIG. 10. Log-log plot of finite-lattice susceptibility and true susceptibility vs the linear size of the lattice L at $T_c=1.052$ for $J_1=1.0$, $J_3=2.0$, and $J_2=0.6$. The solid line is obtained by fitting the data to Eq. (16).

$$\gamma = \nu(2-\eta) = \beta(\delta-1), \tag{30}$$

on the other hand the Rushbrook scaling law $(\alpha+2\beta+\gamma=2)$ is satisfied for all sets of exponents within the computational errors.

In order to check the values of specific-heat anomaly exponents, we also estimated them independently, using size dependence of the specific heat at measured critical temperatures according to Eq. (17). For this purpose we used the least-squares method to find the best value of α/ν to fit the heat capacity data at T_c. The plot of such efforts has been represented in Figs. 12 and 13 for $J_2=0.7$ and $J_2=0.8$, respectively, which resulted in $\alpha/\nu=45(2)$ for $J_2=0.7$ and $\alpha/\nu=0.39(1)$ for $J_2=0.8$. Knowing the obtained values of ν, we find $\alpha=0.36(2)$ for $J_2=0.7$ and $\alpha=0.33(1)$ for $J_2=0.8$. These results are in very good agreement with the values obtained from Josephson scaling law.

One can see from Table I that the critical exponents for $J_2=0.6$ are close to the two-dimensional Ising model for which the exact exponents are $\alpha=0$, $\nu=1.0$, $\beta=0.125$, γ

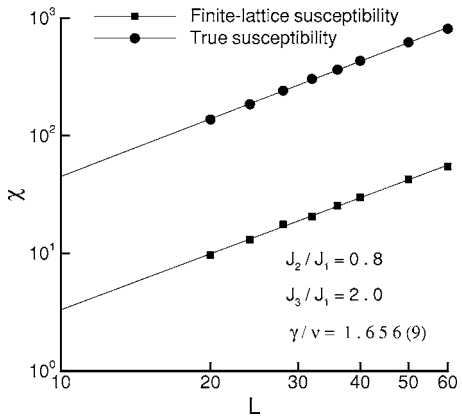

FIG. 11. Log-log plot of finite-lattice susceptibility and true susceptibility vs the linear size of the lattice L at $T_c=1.257$ for $J_1=1.0$, $J_3=2.0$, and $J_2=0.8$. The solid line is obtained by fitting the data to Eq. (16).

TABLE I. The critical temperatures and static critical exponents for $\frac{J_2}{J_1}=0.6,0.7,0.8,0.9,1.0$ and $\frac{J_3}{J_1}=2.0$, derived from finite-size scaling (see the text).

J_2/J_1	T_c	ν	β	γ	α	δ	η
0.6	1.051(1)	1.01(3)	0.144(14)	1.73(6)	−0.02(6)	13.0(1.6)	0.282(8)
0.7	1.164(1)	0.806(9)	0.143(9)	1.31(3)	0.39(2)	10.1(9)	0.370(30)
0.8	1.257(1)	0.837(8)	0.142(5)	1.39(1)	0.32(2)	10.8(4)	0.344(9)
0.9	1.342(1)	0.886(3)	0.156(5)	1.46(1)	0.23(1)	10.3(4)	0.35(1)
1.0	1.423(1)	0.888(3)	0.150(4)	1.48(2)	0.22(2)	10.8(4)	0.33(1)

$=1.75$, $\delta=15$, and $\eta=0.25$. So $J_2=0.6$ is the onset of 2D-Ising behavior. By increasing the threefold coupling constant, the thermal exponents α and ν differ dramatically from that of 2D-Ising value. Heat capacity anomaly exponent α gets its maximum value ($\alpha=0.39$) for $J_2=0.7$ and then decreases to 0.22 for $J_2=1.0$. The critical exponents for $J_2=0.9$ and $J_2=1.0$ are equal up to the simulation errors, hence these two belong to the same universality class.

The specific-heat exponent corresponding to $J_2=0.8$ [$\alpha=0.32(2)$] is the closest one to experimentally observed values ($\alpha=0.31\pm0.03$). To investigate the sensibility of the critical exponents to intensity of hexatic-threefold couplings, we also measured the critical exponents for the coupling set $J_1=1.0$, $J_2=0.8$, and $J_3=1.0$. The static critical exponents obtained for this set of couplings are as $\alpha=0.31(3)$, $\nu=0.845(15)$, $\beta=0.13(2)$, $\gamma=1.43(3)$, $\delta=12.2(1.9)$, and $\eta=0.30(1)$. As we see again the heat capacity exponent is in excellent agreement with experimental value.

IV. CONCLUSION

In summary, using the optimized Monte Carlo simulation based on multihistogram and Wolff's embedding methods, we investigated the critical properties associated with a Hamiltonian containing two coupled XY order parameters (indicating a hexatic field with sixfold symmetry and a hidden order parameter with threefold symmetry) in two dimensions. By presenting this model we aim to model the transition from smectic-*A* to hexatic-*B* in some liquid crystal compounds for which this transition is not accompanied by the appearance of herringbone packing of molecules in smectic planes. Unlike the Bruinsma and Aeppli model, which possess the three state Potts symmetry (because they considered the short range herringbone correlations and so attributed a twofold symmetric order parameter to it), the interplaying of hexatic and threefold hidden orderings, in our model, results in a coupling term with Ising symmetry.

The order of transition for some values of coupling in coupling constants space, for which both kinds of orderings establish simultaneously, were investigated and all of them were found to be second order. All the static critical exponents were derived by finite-size analysis for these range of couplings. Our simulations indicate clear deviations from two-dimensional Ising behavior and nonuniversal characteristics by varying the coupling constants along the transition line between isotropic and locked phases. Considering the J_1 and J_2 to be the hexatic and threefold couplings, respectively, and J_3 as the coupling between hexatic and threefold order parameters, we found that for the ratio $J_2/J_1=0.6$ (the onset of transition from disorder to locked phase), the critical behavior is Ising-like while by increasing the threefold coupling the critical exponents begin to deviate from those of Ising values and finally reach a new universality class corresponding to $J_2/J_1=0.9$ and $J_2/J_1=1.0$ for which the exponents remain unchanged. Surprisingly for some values of

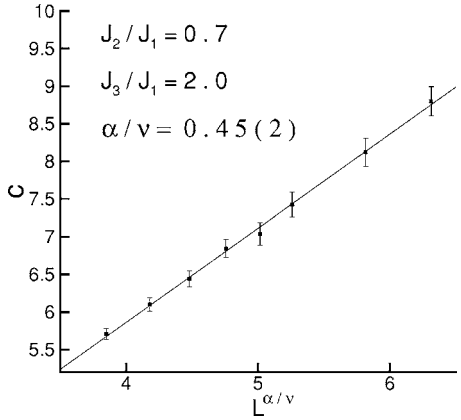

FIG. 12. Size dependence of specific heat at $T_c=1.164$ for $J_1=1.0$, $J_3=2.0$, and $J_2=0.7$. The solid line is obtained by fitting the data to Eq. (17).

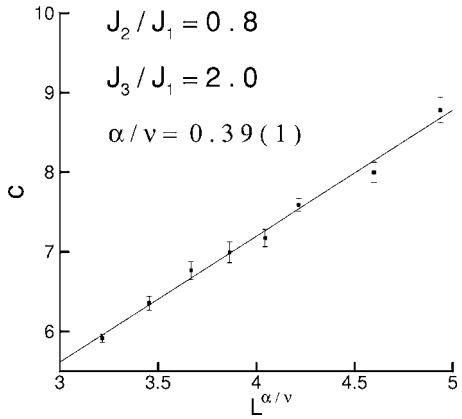

FIG. 13. Size dependence of specific heat at $T_c=1.257$ for $J_1=1.0$, $J_3=2.0$, and $J_2=0.8$. The solid line is obtained by fitting the data to Eq. (17).

threefold couplings between these two limits, i.e, $J_2/J_1 \sim 0.8$ and some values of coupling term, i.e, $J_3/J_1=2.0, 1.0$, the heat capacity exponents show very good agreement with experimentally observed values for two-layered free-standing films of some liquid crystal compounds exhibiting smectic-*A*–hexatic-*B* transition.

The violation of the universality hypothesis has also occurred in some models such as the eight-vertex model solved by Baxter [46] and Ising model with nearest and next nearest neighbor interactions [48]. It has been shown by Kadanoff and Wegner that the existence of marginal operators is a necessary condition for the appearance of continuously varying critical exponents [47]. Whether or not the transitions, studied in this work, are indicating the existence of some marginal operators or just a crossover behavior is an open problem and requires more theoretical investigations based on renormalization group theory.

Our results suggest that the coupling of hexatic ordering to a continuous order parameter, with threefold symmetry, is able to give a plausible description for large specific-heat anomaly exponents of Sm*A*–Hex*B* transition in some liquid crystal compounds, despite the absence of herringbone ordering in their hexatic phases. The confirmation of this idea requires the similar simulation in three dimensions and is the subject of our current research. Experimentally, measuring other static critical exponents rather than heat capacity exponent in thin film samples are also needed to check the validity of this model.

Apart from hexatic transitions in smectic liquid crystals, this study may also shed light on the wide context of coupled XY models where unusual critical behavior often occurs and we finally hope that our work will motivate further theoretical, numerical, and experimental investigations of these very interesting problems.

ACKNOWLEDGMENTS

We would like to thank Hadi Akbarzadeh for letting us use his computational facilities. We also appreciate Mehdi Safa for critically reading this paper.

[1] J. M. Kosterlitz and D. J. Thouless, J. Phys. C **6**, 1181 (1973); J. M. Kosterlitz, *ibid.* **7**, 1046 (1974).
[2] B. I. Halperin and D. R. Nelson, Phys. Rev. Lett. **41**, 121 (1978); D. R. Nelson and B. I. Halperin, Phys. Rev. B **19**, 2457 (1979).
[3] A. P. Young, Phys. Rev. B **19**, 1855 (1979).
[4] K. J. Strandburg, Rev. Mod. Phys. **60**, 161 (1988).
[5] R. J. Birgeneau and J. D. Lister, J. Phys. (Paris), Lett. **39**, L339 (1978).
[6] R. Pindak, D. E. Moncton, S. C. Davey, and J. W. Goodby, Phys. Rev. Lett. **46**, 1135 (1981); J. W. Goodby and R. Pindak, Mol. Cryst. Liq. Cryst. **75**, 233 (1981); S. C. Davey, J. Budai, J. W. Goodby, R. Pindak, and D. E. Moncton, Phys. Rev. Lett. **53**, 2129 (1984).
[7] C. C. Huang and T. Stobe, Adv. Phys. **42**, 343 (1993), and references therein; T. Stobe and C. C. Huang, Int. J. Mod. Phys. B **9**, 2285 (1995).
[8] C. C. Huang *et al.*, Phys. Rev. Lett. **46**, 1289 (1981).
[9] T. Pitchford, G. Nounesis, S. Dumiongrattana, J. M. Viner, C. C. Huang, and J. W. Goodby, Phys. Rev. A **32**, 1938 (1985).
[10] J. C. LeGuillou and J. Zinn Justin, J. Phys. (Paris), Lett. **46**, L137 (1985).
[11] H. Haga, Z. Kutnjak, G. S. Iannacchione, S. Qian, D. Finotello, and C. W. Garland, Phys. Rev. E **56**, 1808 (1997).
[12] H. Haga and C. W. Garland, Phys. Rev. E **57**, 603 (1998).
[13] Z. Kutnjak and C. W. Garland, Phys. Rev. E **57**, 3015 (1998).
[14] T. Stoebe, C. C. Huang, and J. W. Goodby, Phys. Rev. Lett. **68**, 2944 (1992).
[15] A. J. Jin, M. Veum, T. Stoebe, C. F. Chou, J. T. Ho, S. W. Hui, V. Surendranath, and C. C. Huang, Phys. Rev. Lett. **74**, 4863 (1995).
[16] A. J. Jin, M. Veum, T. Stoebe, C. F. Chou, J. T. Ho, S. W. Hui, V. Surendranath, and C. C. Huang, Phys. Rev. E **53**, 3639 (1996).
[17] R. Bruinsma and G. Aeppli, Phys. Rev. Lett. **48**, 1625 (1982).
[18] M. J. P. Gingras, P. C. W. Holdworth, and B. Bergersen, Europhys. Lett. **9**, 539 (1989); Phys. Rev. A **41**, 3377 (1990); **41**, 6786 (1990).
[19] M. J. P. Gingras, P. C. W. Holdworth, and B. Bergersen, Mol. Cryst. Liq. Cryst. **204**, 177 (1991).
[20] M. Kohandel, M. J. P. Gingras, and J. P. Kemp, Phys. Rev. E **68**, 041701 (2003).
[21] I. M. Jiang, S. N. Huang, J. Y. Ko, T. Stoebe, A. K. Jin, and C. C. Huang, Phys. Rev. E **48**, R3240 (1993).
[22] I. M. Jiang, T. Stoebe, and C. C. Huang, Phys. Rev. Lett. **76**, 2910 (1996).
[23] R. Ghanbari and F. Shahbazi, Phys. Rev. E **72**, 021709 (2005).
[24] G. Aeppli and R. Bruinsma, Phys. Rev. Lett. **53**, 2133 (1984).
[25] A. Aharony, R. J. Birgeneau, J. D. Brock, and J. D. Litster, Phys. Rev. Lett. **57**, 1012 (1986).
[26] J. V. Selinger, J. Phys. (Paris) **49**, 1387 (1988).
[27] A. D. Défontaines and J. Prost, Phys. Rev. E **47**, 1184 (1993).
[28] J. Villain, J. Phys. C **10**, 4793 (1977); R. F. Voss and R. A. Webb, Phys. Rev. B **25**, 3446 (1982); R. A. Webb, R. F. Voss, G. Grinstein, and P. M. Horn, Phys. Rev. Lett. **51**, 690 (1983); S. Teitel and C. Jayaprakash, *ibid.* **51**, 1999 (1983); Phys. Rev. B **27**, 598 (1983); M. Y. Choi and S. Doniach, *ibid.* **31**, 4516 (1985); T. C. Halsey, J. Phys. C **18**, 2437 (1985); P. Martinoli and Ch. Leemann, J. Low Temp. Phys. **118**, 699 (2000); X. S. Ling *et al.*, Phys. Rev. Lett. **76**, 2989 (1996); **77**, 410(E) (1996); D. Loison and P. Simon, Phys. Rev. B **61**, 6114 (2000).
[29] S. Miyashita and H. Shiba, J. Phys. Soc. Jpn. **53**, 1145 (1984); D. H. Lee, J. D. Joannopoulos, J. W. Negele, and D. P. Landau, Phys. Rev. Lett. **52**, 433 (1984); (unpublished).
[30] N. Parga and J. E. Himbergen, Solid State Commun. **35**, 607 (1980).
[31] T. Garel and S. Doniach, J. Phys. C **13**, L887 (1980).
[32] W. Janke and H. Kleinert, Phys. Rev. Lett. **57**, 279 (1986).
[33] E. Granato, J. M. Kosterlitz, J. Lee, and M. P. Nightingale,

Phys. Rev. Lett. **66**, 1090 (1991); M. P. Nightingale, E. Granato, and J. M. Kosterlitz, Phys. Rev. B **52**, 7402 (1995).
[34] E. Granato, J. M. Kosterlitz, and J. Poulter, Phys. Rev. B **33**, 4767 (1986).
[35] U. Wolff, Phys. Rev. Lett. **62**, 361 (1989); Nucl. Phys. B **322**, 759 (1989).
[36] R. H. Swendsen and J. S. Wang, Phys. Rev. Lett. **58**, 86 (1987).
[37] P. Tamayo, R. C. Brower, and W. Klein, J. Stat. Phys. **58**, 1083 (1990).
[38] D. Kandel and E. Domany, Phys. Rev. B **43**, 8539 (1991).
[39] K. Chen, A. M. Ferrenberg, and D. P. Landau, Phys. Rev. B **48**, 3249 (1993).
[40] P. Peczak, A. M. Ferrenberg, and D. P. Landau, Phys. Rev. B **43**, 6087 (1991).
[41] A. M. Ferrenberg and R. H. Swendsen, Phys. Rev. Lett. **63**, 1195 (1989).
[42] M. N. Barber, *Phase Transitions and Critical Phenomena*, edited by C. Domb and J. L. Lebowitz (Academic, New York, 1983), Vol. 8, p. 145.
[43] D. P. Landau and K. Binder, *A Guide to Monte Carlo Simulations in Statistical Physics* (Cambridge University Press, Cambridge, England, 2000).
[44] M. S. S. Challa, D. P. Landau, and K. Binder, Phys. Rev. B **34**, 1841 (1986).
[45] J. Lee and J. M. Kosterlitz, Phys. Rev. B **43**, 3265 (1991).
[46] R. J. Baxter, Ann. Phys. (N.Y.) **70**, 193 (1972); *Exactly Solved Models in Statistical Mechanics* (Academic Press, London, 1982).
[47] L. P. Kadanoff and F. J. Wegner, Phys. Rev. B **4**, 3989 (1971).
[48] N. W. Dalton and D. W. Wood, J. Math. Phys. **10**, 1271 (1969); C. Fan and F. Y. Wu, Phys. Rev. **179**, 560 (1969); R. W. Gibbert, J. Math. Phys. **10**, 1026 (1969); M. Nauenberg and B. Nienhuis, Phys. Rev. Lett. **33**, 944 (1974); J. M. J. van Leeuwen, *ibid.* **34**, 1056 (1975); M. P. Nightigale, Phys. Lett. **59**, 486 (1977); R. H. Swendsen and S. Krinsky, Phys. Rev. Lett. **43**, 177 (1979); T. W. Burkardt, Z. Phys. B **29**, 129 (1978); D. P. Landau, Phys. Rev. B **21**, 1285 (1980); K. Binder and D. P. Landau, *ibid.* **21**, 1941 (1980).